Oligonucleotides Hot Paper

How to cite:
International Edition: doi.org/10.1002/anie.202116783
German Edition: doi.org/10.1002/ange.202116783

Tuning Exciton Coupling of Merocyanine Nucleoside Dimers by RNA, DNA and GNA Double Helix Conformations

Julia Dietzsch, David Bialas, Johannes Bandorf, Frank Würthner, and Claudia Höbartner**

Abstract: *Exciton coupling between two or more chromophores in a specific environment is a key mechanism associated with color tuning and modulation of absorption energies. This concept is well exemplified by natural photosynthetic proteins, and can also be achieved in synthetic nucleic acid nanostructures. Here we report the coupling of barbituric acid merocyanine (BAM) nucleoside analogues and show that exciton coupling can be tuned by the double helix conformation. BAM is a nucleobase mimic that was incorporated in the phosphodiester backbone of RNA, DNA and GNA oligonucleotides. Duplexes with different backbone constitutions and geometries afforded different mutual dye arrangements, leading to distinct optical signatures due to competing modes of chromophore organization via electrostatic, dipolar, π–π-stacking and hydrogen-bonding interactions. The realized supramolecular motifs include hydrogen-bonded BAM–adenine base pairs and antiparallel as well as rotationally stacked BAM dimer aggregates with distinct absorption, CD and fluorescence properties.*

Introduction

The programmable nature of Watson–Crick base pairing in DNA offers precise control over the arrangement of chromophores and nanometer-scaled objects for the design of intelligent materials, with functions beyond the storage of genetic information. Fluorescent nucleoside analogs[1] that retain hydrogen-bonding properties or provide enhanced π–π-stacking abilities enabled the investigation of RNA/DNA folding landscapes, ligand and protein interactions, the detection of RNA modifications, and have found applications as fluorescent hybridization probes. For example, the merocyanine thiazol orange was extensively used as base surrogate[2] and formed the basis for forced intercalation (FIT) probes[3] and FRET-based RNA "traffic lights",[4] and its fluorogenic behavior was also exploited in the Mango family of light-up aptamers.[5] The incorporation of multiple chromophore units into nucleic acids has previously enabled the precise arrangement of e.g. polycyclic aromatic hydrocarbons (including naphthalene, phenanthrene, pyrene),[6] biphenyl,[7] binaphthyl,[8] tetraphenylethylene,[9] perylene bisimides,[10] cyanines,[11] squaraines,[12] porphyrins[13] and other dyes for the design of novel functions.[14] For example, Cy3 and Cy5 were covalently incorporated via alkyl linkers in DNA duplexes and shown to cause the proximity-induced formation of J- and H-like aggregates.[15] Cofacial π–π-stacking into H-aggregates is also a common feature observed for dipolar merocyanines driven by electrostatic dipole-dipole interactions that has been utilized for the formation of defined self-assembled dye stacks,[16] extended supramolecular polymers,[17] and the stepwise folding of merocyanine peptide foldamers in solvents of low polarity.[18] Here, we investigated the interactions of merocyanines (MC) with barbituric acid acceptor groups in the aqueous environment, by incorporation as nucleobase analogues in three different nucleic acid backbones, namely RNA, DNA and GNA (Figure 1a). Glycol nucleic acid (GNA) is an artificial nucleic acid with nucleobases connected to a 1,2-propanediol phosphodiester backbone, capable of forming antiparallel Watson–Crick base-paired duplexes with high thermal stability.[19] The helix geometry of GNA duplexes is distinct from canonical A- and B-form nucleic acids,[20] with a rise of 3.8 Å/bp and 16 bp/turn, in contrast to 2.6 Å/bp (11 bp/turn) in A-form RNA and 3.4 Å/bp (10 bp/turn) in B-form DNA. We provide a side-by-side comparison of the three double-helical supramolecular elements[21] containing the same sequence but differing in their backbone constitutions. Replacing only the nucleobase by the chromophore but maintaining the nucleosidic backbone enabled us to study how the assembly and MC dimerization are governed by the structure of the antiparallel nucleic acid duplexes. We found that the degree of exciton coupling in MC nucleic acids, as well as the magnitude of folding-induced fluorescence activation or deactivation are not only a result of the different backbone conformations of the RNA, DNA or GNA double helix, but also depend on the relative position of the MC in the nucleic acid sequence (downstream, upstream or directly opposite the second MC).

[*] J. Dietzsch, Dr. D. Bialas, J. Bandorf, Prof. Dr. F. Würthner, Prof. Dr. C. Höbartner
Institute of Organic Chemistry, University of Würzburg (Germany)
E-mail: wuerthner@uni-wuerzburg.de
claudia.hoebartner@uni-wuerzburg.de
Dr. D. Bialas, Prof. Dr. F. Würthner, Prof. Dr. C. Höbartner
Center for Nanosystems Chemistry, University of Würzburg
Am Hubland, 97074 Würzburg (Germany)

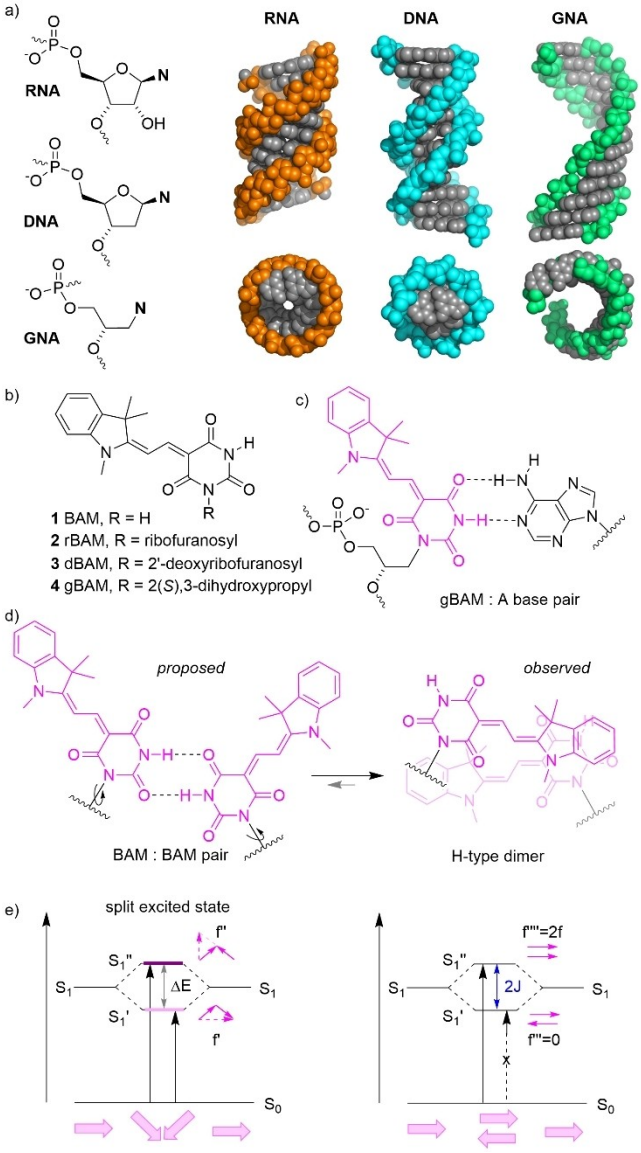

Figure 1. a) Monomer constitutions and helix conformations of RNA, DNA and GNA. Side view and top view of 12-bp duplex models in ideal A-form (RNA) and B-form (DNA) helix geometry, 12-bp GNA model (according to pdb 2jja). b) Barbituric acid merocyanine **1** and the rBAM, dBAM and gBAM nucleoside analogs **2**, **3** and **4**. c) Base pairing with adenine. d) Competition between H-bonding and antiparallel dipolar stacking of two BAM facing each other in a duplex. e) Schematic exciton state diagrams for twisted (oblique) (left) and antiparallel (right) MC dimers. S_0 ground state, S_1 first excited state, J exciton coupling energy, f (f' f'' f''' f'''') oscillator strength of monomer (and the respective dimers).

Results and Discussion

Concept

We used the barbituric acid merocyanine (BAM) **1**[22] as nucleobase surrogate, inspired by its structural similarity to indolenine-derived hemicyanines described for the fluorogenic detection of natural 5-formylpyrimidine nucleotides in DNA and RNA,[23] and by previous[24] and recent[25] research on hydrogen bond-directed supramolecular assemblies of dipolar barbituric acid merocyanines. Here we designed and synthesized the ribonucleoside (rBAM) **2**, 2′-deoxyribonucleoside (dBAM) **3**, and the acyclic (*S*)-glycol nucleoside analog (gBAM) **4** (Figure 1b). Their incorporation into the nucleic acid phosphodiester backbones of RNA, DNA or GNA, respectively, should result in a hybridization-competent orientation of the barbituric acid head group for hydrogen bonding interactions upon duplex formation. A Watson–Crick like base pair with adenosine (Figure 1c) or a pyrimidine-pyrimidine base pair with a second BAM residue (Figure 1d) would orient the chromophores towards the major groove. Alternatively, rotation around the glycosidic bond may orient the hydrophobic indolenine part towards the center of the helix to facilitate π–π stacking with neighboring nucleotides and the formation of H-type dimers, resulting in coupling of the transition dipole moments and split excited states. Such different orientations produce distinct optical features (Figure 1e) that can be observed by absorption and CD spectroscopy and interpreted according to the molecular exciton theory.

Synthesis

The nucleosides rBAM (**2**) and dBAM (**3**) were prepared by condensation of barbituric acid β-D-ribofuranosides **5** and **6**, respectively, with the aldehyde **7**, and were then converted to 5′-*O*-*DMT*-protected 3′-cyanoethyl phosphoramidites **8** and **9** (Figure 2). The corresponding GNA analogue was prepared from **1** by base-catalyzed epoxide ring-opening of *DMT*-protected (*R*)-glycidol, in analogy to established syntheses of GNA nucleosides,[26] and transformed to phosphoramidite **10** upon treatment with *CEP*-Cl.

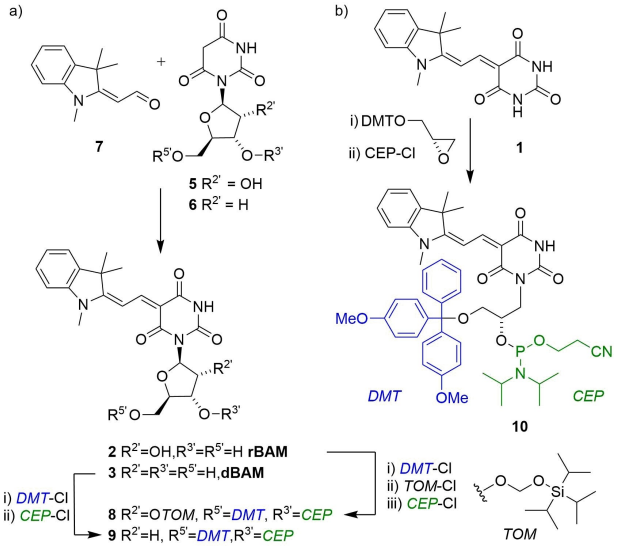

Figure 2. a) Synthesis of rBAM and dBAM phosphoramidites **8** and **9**. b) Synthesis of gBAM phosphoramidite **10**. *DMT*-Cl = 4,4′-dimethoxytrityl chloride, *TOM*-Cl = triisopropylsilyloxymethyl chloride, *CEP*-Cl = 2-cyanoethyl *N*,*N*-diisopropyl chlorophosphoramidite.

A series of BAM-containing RNA, DNA and GNA oligonucleotides were prepared by solid-phase synthesis on controlled pore glass (CPG) (Table S1). Standard phosphoramidites were used for DNA, and 2′-*O*-TOM protected ribonucleotides for RNA. GNA was prepared in DMT-on mode on phosphate CPG. Cleavage from the solid support and deprotection was achieved under mild conditions with aqueous ammonia at 37 °C for 12 h, followed by cleavage of the terminal DMT group with acetic acid. Purification by denaturing PAGE afforded free RNA and DNA with terminal hydroxyl groups, and GNA oligonucleotides with 3′-terminal phosphate groups in high quality and good yields. HPLC chromatograms and HR-ESI-MS data are given in the Supporting Information.

Hybridization and Melting Studies

Complementary single strands were mixed in equimolar ratio and the influence of rBAM, dBAM and gBAM on the thermodynamic duplex stability of RNA, DNA and GNA double helices, respectively, was investigated by concentration-dependent thermal melting experiments monitored by UV absorption at 260 nm (Table 1). The GNA duplex containing a single BAM:A base pair (**G1**) was only moderately destabilized compared to the unmodified duplex **G0** (T_m reduced by 5 °C), and gBAM retained the ability of mismatch discrimination similar to thymidine (i.e. further strongly reduced T_ms were observed when BAM was placed opposite G, C, or T, see Table S4). In contrast, BAM:A base pairs were more strongly disfavored in RNA and DNA duplexes, resulting in 16 °C (**R1**) or 10 °C (**D1**) reduced melting temperatures compared to the unmodified references (**R0**, **D0**), and duplexes with mismatched BAM showed similarly reduced T_ms (Tables S2 and S3), indicating that rBAM and dBAM do not maintain the optimal conformation for Watson-Crick base pairing. Interestingly, incorporation of a second BAM:A pair downstream ("after" the first one, in **R2a**) or upstream ("before" the first one, in **R2b**) was well tolerated and reduced the T_ms by only 2 °C compared to **R1**. In the DNA series, incorporation of a second BAM in **D2a** and **D2b** even partially rescued the drop in melting temperatures caused by the first BAM. Surprisingly, the most pronounced stabilizing effect upon MC dimer formation was observed when two dBAM nucleosides faced each other in **D2c**, which had a T_m of 40.4 °C, which is only 3.2 °C lower than the unmodified DNA. In strong contrast, **G2c** showed the lowest T_m in the double-modified GNA series (11.6 °C lower than unmodified, and 3.8/7.3 °C lower than **G2a**/**G2b**).

Table 1: Melting temperatures of RNA, DNA and GNA duplexes from thermal denaturation monitored by UV absorption at 260 nm.

No 5′-NNN-3′ No 3′-NNN-5′	RNA[b]	T_m[c]	DNA[b]	T_m[c]	GNA[b]	T_m[c]
S1 GATGATAGCTAG[a] S2 CTACTATCGATC	R0	54.4	D0	43.6	G0	67.0
S1 GATGATAGCTAG S3 CTACTA**X**CGATC	R1	38.2	D1	33.5	G1	61.9
S4 GATGA**X**AGCTAG S3 CTACTA**X**CGATC	R2a	35.9	D2a	34.9	G2a	59.2
S4 GATGA**X**AGCTAG S5 CTAC**X**ATCGATC	R2b	36.0	D2b	37.2	G2b	62.7
S4 GATGA**X**AGCTAG S6 CTACT**X**TCGATC	R2c	39.2	D2c	40.4	G2c	55.4

[a] sequences for DNA series, see Tables S1–S4 for RNA and GNA. X indicates the position of the modification (X = rBAM, dBAM, gBAM, respectively). [b] Letter indicates backbone constitution. R = RNA; D = DNA; G = GNA; numbers indicate number of chromophores in the duplex. Lower case letters indicate relative direction of second X in duplex: *a* = "after" (downstream), *b* = "before" (upstream), *c* = "across". [c] Melting temperature in °C at 5 μM strand concentration in 100 mM NaCl, 10 mM phosphate buffer, pH 7.0. Melting curves and van't Hoff plots for five concentrations (1–20 μM) are shown in the Supporting Information.

UV/Vis Absorption and CD spectroscopy

To interpret these results, it is important to note that both the hyperchromicity at 260 nm and the CD spectra in the UV spectral range indicated that the double helical features remained unperturbed or were only slightly perturbed by the nucleobase surrogates. Watson–Crick base pairing in the DNA duplex was further confirmed by recording ^{1}H NMR spectra, showing characteristic signals in the imino proton region (11–14 ppm, Figure S1). The melting curves were also monitored at 460 nm and the inflection points were almost superimposable to the ones determined at 260 nm. This observation reflects a high degree of cooperativity in the duplex and indicates that the UV/Vis spectra reflect chromophore interactions upon hybridization of the single strands. The bisignate features of the CD spectra in the visible range can therefore be attributed to the interacting MC dyes, which are known to show geometry and distance dependent exciton coupling upon formation of MC dimers.[16a] Interestingly, the magnitude and the sign of the Cotton effect varied significantly for the three different helix conformations. While all three double-modified RNA duplexes showed positive CD couplets of comparable magnitude, the sign of the CD couplet switched with the relative orientation of the chromophores in **D2a** compared to **D2b** and **D2c**. In other words, the bisignate CD signal in the DNA duplexes **D2b** and **D2c** showed opposite chirality to the analogous architectures in RNA duplexes **R2b** and **R2c**. This result may be rationalized by one possible orientation of the chromophore dimer in the A-form helix, which is characterized by a strong base-pair inclination and deep major groove, while Watson–Crick base pairs are essentially perpendicular to the helix axis in a B-form duplex allowing more freedom for relative dye orientations. A similar observation of inverted Cotton effects was previously reported for thiazol orange incorporated via a threoninol linkage into DNA and RNA duplexes.[27] In the GNA series, the strongest CD effect was observed for **G2a**, while **G2c** showed a negative CD couplet of smaller intensity and the CD spectrum of **G2b** showed additional fine structures, which are not easily rationalized in the absence of a 3D

structure. Nevertheless, the trends observed in the CD spectra are consistent with the UV/Vis absorption spectra, which also showed orientation-dependent exciton coupling in double BAM-modified RNA, DNA and GNA duplexes (Figure 3).

At 80 °C, all duplexes were denatured and the absorption spectra of the single stands resembled the BAM monomer absorption in all cases. At 20 °C, the spectra showed pronounced exciton coupling of two BAM moieties in the A-form helix when they were oriented in the downstream orientation **R2a**, but much less in the upstream orientation **R2b**. A sharp absorption peak in **R2a** with a maximum at 436 nm was observed, which is blue-shifted by 30 nm compared to the single strand. The spectrum also contained a shoulder at shorter wavelength (415 nm) and a bathochromically shifted second band at 473 nm of about one third of the maximum intensity. At 40 °C, two bands appeared of approximately equal height, consistent with a T_m of 36 °C, at which 50 % of the duplex is dissociated. In contrast to **R2a**, the absorption spectrum of **R2b** at 20 °C showed less separated bands, despite a similar melting temperature, suggesting a different exciton coupling strengths, which is also reflected in the smaller $\Delta\lambda$ in the CD signature of **R2b** (36 nm, compared to 56 nm in **R2a**). Interestingly, an inverted situation was observed in the absorption spectra of the B-form DNA helix: strong MC coupling was seen in the upstream orientation **D2b** (showing an absorption spectrum similar to **R2a**), while **D2a** was comparable to **R2b**. In the GNA duplex, the chromophores barely interacted in the downstream orientation in duplex **G2a**, but duplex **G2b** again showed an enhanced hypsochromically shifted absorption maximum at 437 nm, which disappeared upon thermal denaturation. This suggests that the chromophores entertain dipolar stacking interactions in **G2b** but not in **G2a**, which is also consistent with the higher melting temperature of **G2b**.

The spectra of duplexes with chromophores facing each other at opposite positions also showed drastic differences between furanosyl and acyclic backbones (Figure 3c). The UV/Vis spectra of the RNA and DNA duplexes **R2c** and **D2c** indicated the formation of H-type dimers with a band at 435 nm, and shoulders at 415 and 472 nm. In strong contrast to these duplexes with native ribose backbones, the spectrum of the GNA duplex **G2c** closely resembled the

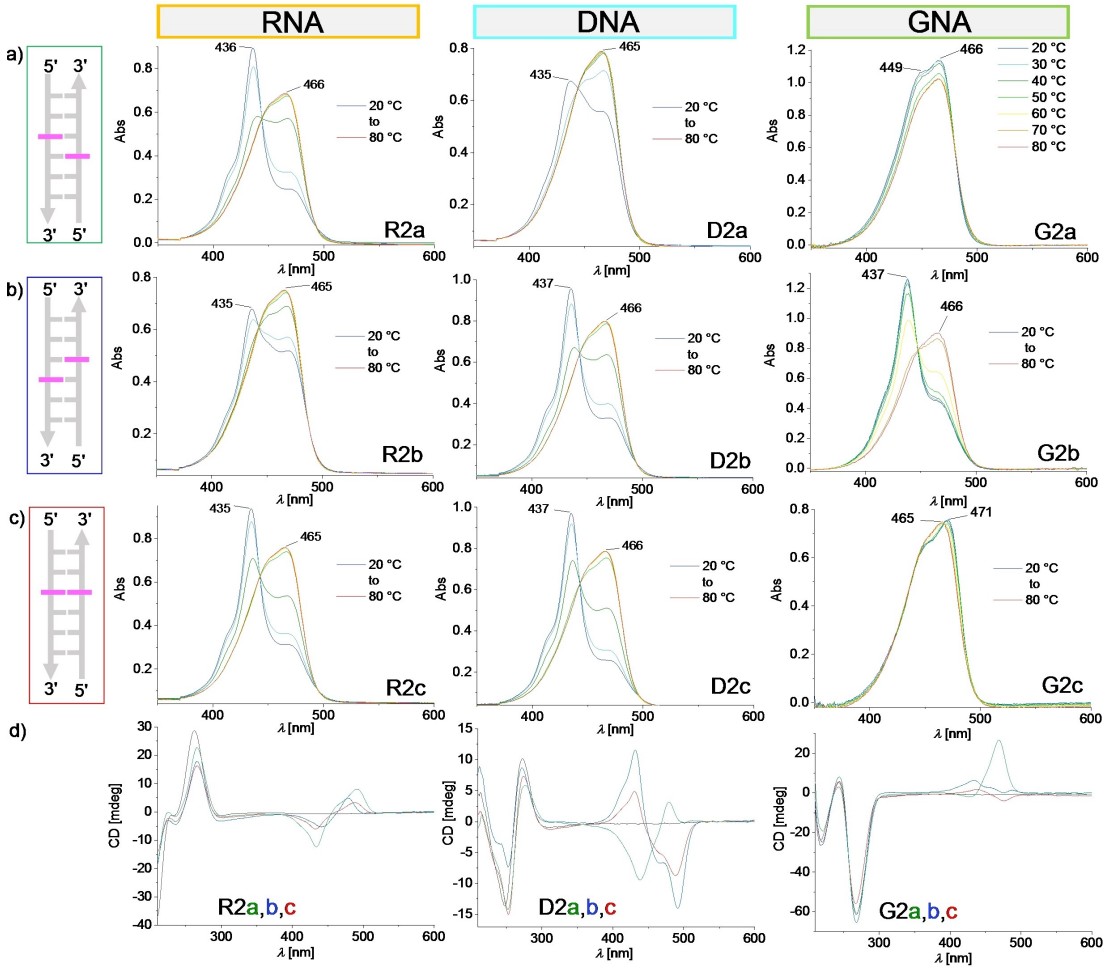

Figure 3. UV/Vis absorption spectra (a)–(c) and CD spectra (d) of duplexes containing two BAM nucleosides. Left column RNA, middle column DNA, right column GNA, a) downstream (R/D/G2a), b) upstream (R/D/G2b), and c) opposite (R/D/G2c) orientations. UV/Vis: temperature dependent spectra between 20 and 80 °C, CD at 20 °C; all: 5 μM duplex in 100 mM NaCl, 10 mM Na phosphate buffer, pH 7.0, $d = 1$ cm.

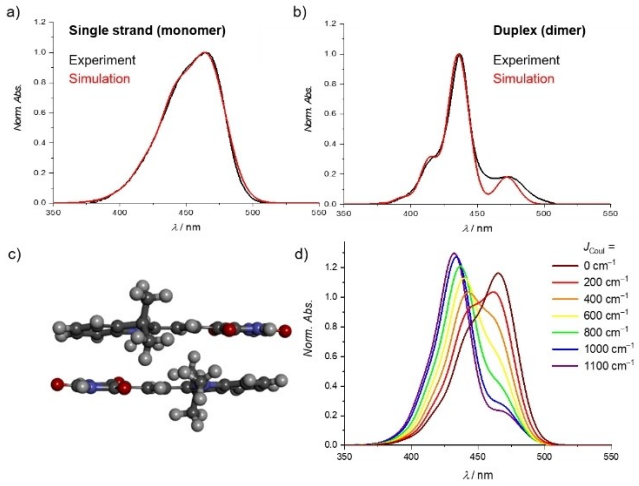

Figure 4. Simulated absorption spectra (red) of BAM monomer (a) and geometry-optimized antiparallel BAM dimer (b, without nucleic acid), in comparison to experimental spectra (black) of single strands (**D2c** at 90 °C) and duplex (**D2c** at 10 °C). c) Geometry-optimized structure (DFT) of antiparallel BAM dimer in the absence of any nucleic acid environment. d) Simulated absorption spectra of BAM dimer with different coupling strengths. Transition energy: $E_g = 21\,400\ cm^{-1}$, vibrational frequency: $\omega_0 = 1200\ cm^{-1}$, Huang–Rhys factor $\lambda^2 = 0.608$, linewidth $\sigma = 780\ cm^{-1}$, maximum number of vibrational quanta: $vib_{max} = 7$.

UV/Vis spectrum of the single strands, and showed only a very small bathochromic shift (5 nm) upon duplex formation, which is consistent with the proposed hydrogen-bonded almost orthogonal orientation in a BAM:BAM base pair (Figure 1d left). This was further supported by comparison with pH-dependent absorption spectra of the free BAM chromophore, which revealed a pK_a of 10.7, and showed moderate solvatochromicity (Figure S2).

In covalent MC dimers[28] and Cy5-labeled DNA scaffolds,[15b,29] spectral features similar to the ones observed for **R2a/c** and **D2b/c** were attributed to partially twisted transition dipole moments and combinations of excitonic coupling and vibronic progression, and confirmed by time-resolved spectroscopy and quantum chemical calculations. To gain deeper insights into BAM dimerization, geometry optimization and simulations of the absorption spectra employing the exciton-vibrational model[30] were performed (details see Supporting Information).The simulated absorption spectra for the BAM monomer and for the geometry-optimized dimer are in good agreement with the experimental absorption spectra at 90 °C (denatured to single strands) and 10 °C (folded duplex), respectively (Figure 4). For the dimer spectrum of **D2c**, a Coulomb coupling of 1100 cm^{-1} and a Huang–Rhys factor of 0.61 have been applied. The simulated dimer spectra with a wider range of coupling energies are shown in Figure 4d, and are reminiscent of the partially folded duplex states at increasing temperatures.

Fluorescence Studies

Incorporation of BAM into oligonucleotides and embedding of the dyes in duplex structures afforded a notable increase of the fluorescence intensity as observed for **R1** ($\Phi_f = 1.6\,\%$) and **D1** ($\Phi_f = 2.9\,\%$) compared to the free BAM chromophore ($\Phi_f < 0.3\,\%$, see Figure S3, S4), likely due to restricting the fast non-radiative decay of the excited state of the free monomer.[2d,31] In particular for the duplexes containing two BAM units, the absorption spectroscopic results are consistent with a preferred orientation of the BAM chromophores in which the hydrophobic indole part is rotated towards the center of the RNA/DNA double helices, implying a *syn* conformation of the glycosidic bond in rBAM and dBAM. However, the presence of the adenosine in the opposite strand and the sterically demanding methyl groups in the indole likely prevent an ideal antiparallel orientation and enforce a twisted MC arrangement, similar to what has been previously observed for stacked thiazol orange dimers resulting in red-shifted fluorescence emission upon DNA hybridization.[2b] The twisted BAM:BAM dimers in **D2c** and **R2c** likewise exhibit distinct fluorescence emission properties in the folded duplex state despite of their antiparallel orientation and H-type coupling. Temperature-dependent fluorescence studies (Figure S6) indicated a pronounced increase in the dimer fluorescence intensity with duplex formation upon decreasing temperature that can be rationalized by the rigidification of BAM in the self-assembled architecture. Here we focus the discussion on **D2c**, but similar results were observed for **R2c**, as well as for **R2a** and **D2b** (Figure S6). As seen in Figure 5a, for **D2c** dimer emission was observed at 540 nm (solid line) and a second transition of lower intensity at 505 nm, which was also red-shifted compared to the emission of the single-modified duplex at 488 nm (dotted lines). The fluorescence quantum yield of **D2c** was 3 % (Figure S4), and an average fluorescence lifetime of 0.8 ns was observed at 540 nm upon excitation at 408 nm (Figure S5), while excitation at 477 nm suggested the presence of an additional component with shorter lifetime. The fluorescence liftetime of the single strand was too short to be accurately determined by TCSPC (< 0.1 ns, see DS6 in Figure S5). The excitation spectrum of the duplex was consistent with the absorption spectrum, and a matrix scan of emission spectra at variable excitation wavelength suggested that the duplex was essentially fully formed in phosphate buffer containing 100 mM NaCl (Figure S7). In contrast, an equimolar mixture of the two complementary single strands in deionized water showed only emission of BAM monomers, but the emergence of the fluorescent BAM dimer was induced by addition of sodium chloride (Figure 5d, e). The NaCl-titration (Figure 5d, e) exhibited a concentration-dependent increase of the excitation band at 433 and the emission band at 540 nm, and a simultaneous decrease at 470 nm (excitation) and 490 nm (emission). The salt-dependent duplex formation was as expected from the counterion condensation theory assuming a mean uniform distribution of condensed ions along the polyelectrolyte upon duplex formation. The spectra of the BAM dimer compared to a BAM monomer in the double

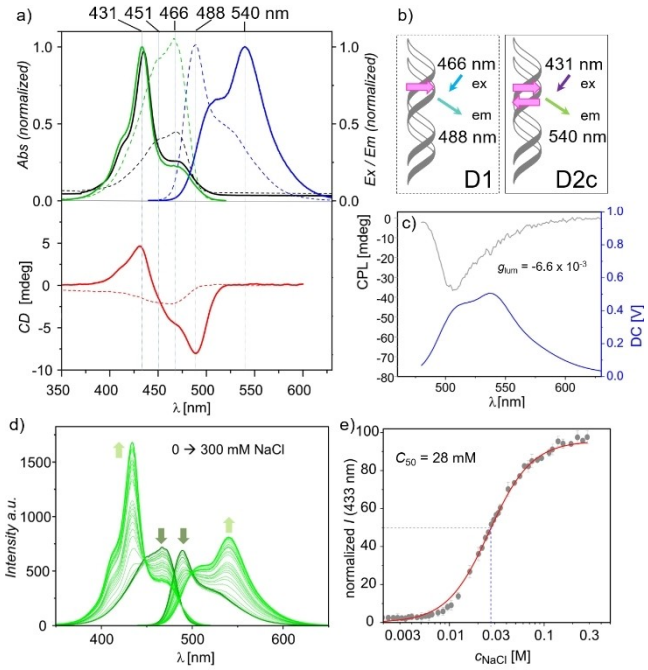

Figure 5. a) Absorption (black), excitation (green), emission (blue) and CD (red) spectra of **D2c** (solid lines) and **D1** (dashed lines). b) Schematic depiction of single- and double-modified DNA duplexes used in (a). c) Circular polarized luminescence (CPL, black) and total luminescence (blue) of **D2c**. Conditions for (a) and (c): 10 mM sodium phosphate buffer pH 7.0, 100 mM NaCl, 20 °C. d) Initiation of fluorescent BAM dimerization by titration of **D2c** (1 μM) in water with increasing concentrations of NaCl. Excitation and emission spectra (λ_{ex} = 420 nm, λ_{em} = 540 nm) up to 300 mM NaCl. e) Normalized intensity at 433 nm vs NaCl concentration (mean ± s.e.m. of three replicates). The red line represents a fit to a multi-binding site model ($x^n/(k^n+x^n)$).

helical environment of the DNA duplex motivated us to probe the extent of chiral fluorescence dissymmetry in the excited state by circularly polarized luminescence (CPL) spectroscopy.[32] Indeed, a CPL signal with negative Cotton effect was detected for **D2c**, with an anisotropy factor g_{lum} of −0.0066 at 505 nm, while the excimer band showed negligible CPL. This observation might be rationalized by differently coupled BAM chromophores, i.e. the prevalence of BAM dyes in an oblique arrangement (CPL active) and an antiparallel arrangement (CPL inactive) as illustrated in Figure 1e.

Interestingly, the fluorescence properties of gBAM-modified duplexes differed significantly from the canonical DNA and RNA duplexes. In general, the observed fluorescence was significantly weaker, which we attribute to a lower degree of rigidification of the BAM units by the GNA oligonucleotide backbone. The GNA structure essentially represents a helical ribbon that does not provide a hydrophobic core for embedding of the dyes like in RNA and DNA helices (compare structural models in Figure 1a). Thus, with a quantum yield of 0.7 %, single-BAM modified **G1** showed weaker fluorescence emission intensity than **R1** and **D1** (Figure S4). The GNA duplexes containing two BAM units also showed weak fluorescence, and no strongly pronounced red-shifted emission maxima were observed (Figure 6). For **G2a** and **G2c** with essentially decoupled chromophores a similar temperature dependence was observed like for **G1**, i.e. a reduced fluorescence intensity upon heating as expected due to enhanced motions at elevated temperature (Figure S6). As a remarkable exception, for **G2b** the fluorescence intensity decreased upon cooling, i.e. hybridization, and this behavior was also observed by titration with NaCl (Figure 6d). Thus, the spatial arrangement of two consecutive BAM:A base pairs in **G2b** resulted not only in the highest thermodynamic stability of all double-modified duplexes, but also in a specific mutual merocyanine arrangement for which the radiative rate is reduced to a larger extent than for the respective RNA and DNA counterparts.

FRET Experiment

Beyond the utilization of BAM-BAM interactions for probing the molecular environment, the fluorescent nature of the BAM chromophore within RNA and DNA may also be utilized for fluorescence resonance energy transfer (FRET) experiments. Toward this goal we here apply 2-aminopurine (2AP), which is a well-established fluorophore for RNA structure probing, but is significantly quenched upon incorporation into DNA or RNA, and further reduced upon hybridization.[33] The overlap of 2AP emission and BAM absorption spectra allowed us to evaluate the FRET

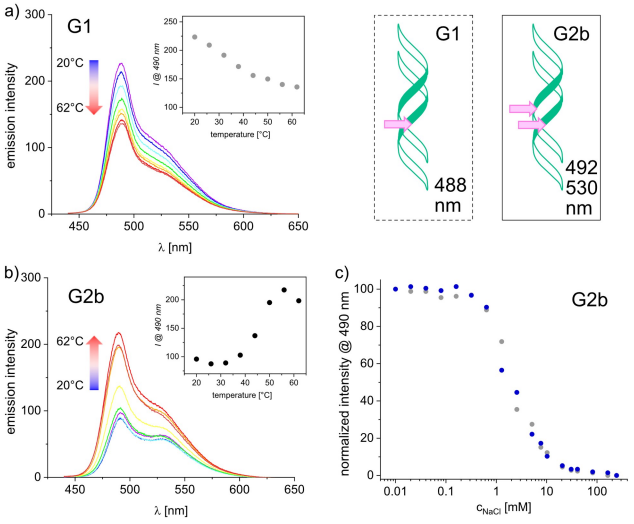

Figure 6. Temperature-dependent fluorescence emission of BAM-modified GNA duplexes **G1** and **G2b**, schematically depicted as elongated helices with attached chromophores. Emission spectra of a) single gBAM-modified duplex **G1** and b) double-modified duplex **G2b** show opposite direction of intensity change (decrease vs increase). Conditions 1 μM duplex in 10 mM sodium phosphate buffer pH 7.0, 100 mM NaCl, 20 °C–62 °C. λ_{ex} = 420 nm. Insets: intensity at 490 nm vs. temperature. c) Initiation of BAM dimerization by titration of **G2b** (1 μM) in water with increasing concentrations of NaCl. Normalized intensity at 490 nm (emission) and 470 nm (excitation) vs. NaCl concentration.

in three duplexes containing 2AP and BAM directly opposite of each other, and one or two base-pairs apart (Figure S8). As expected, the FRET efficiency decreased with increasing donor-acceptor distance, which further confirms that the self-assembly of the dye-labeled oligonucleotides resulted in regular duplex structures.

Conclusion

In this work, we explored the barbituric acid merocyanine (BAM, **1**) as a nucleobase surrogate in RNA, DNA and GNA oligonucleotides, and studied the formation of BAM dimers in the respective duplex structures. The analysis of three different relative chromophore orientations (after (a), before (b), across (c) each other) in the three different backbone constitutions allowed a comprehensive comparison of local exciton couplings in nine structurally defined environments. The results are schematically summarized in Figure 7.

We found that the barbiturate head group of the nucleobase surrogate BAM (**1**) maintains Watson–Crick base pairing ability with adenine in GNA duplexes **G2a** and **G2b** (as in Figure 1c). In contrast, the helical conformations of RNA and DNA duplexes (**R2a/b**, **D2a/b**) favour chromophore reorientations by rotation of the glycosidic bond to maximize co-facial π–π stacking, allowing for dipolar exciton coupling and the formation of fluorescent BAM dimer assemblies with significant circularly polarized emission. Similarly, the placement of two BAMs facing each other in the duplex resulted in H-type dimer formation in DNA and RNA (Figure 1d right for **D2c** and **R2c**), while the orthogonal H-bonded orientation was maintained in GNA (Figure 1d left for **G2c**).

Overall, we have established BAM as a nucleobase analogue that features distinct optical properties in different helical environments. Thus, BAM may find applications as a fluorogenic nucleobase analog with a conformation-sensitive wavelength shift. The emissive dimer formation is likely not restricted to the DNA sequences used in **D2c**, but may be more generally applicable, e.g. to monitor folding of intramolecular nucleic acid structures (e.g. when two BAMs are placed at complementary positions in a stem-loop structure). Indeed, similar bimodal fluorescence enhancement upon exciton coupling as in **D2c** was also observed for **D2b**, and for rBAM dimers in **R2a** and **R2c**, which displayed strong exciton coupling in the absorption spectra (compare Figure 3 and Figure S6). The enhanced fluorescence emission intensity of BAM upon incorporation into RNA oligonucleotides and its spectral overlap with 2-aminopurine makes BAM a promising fluorescent pyrimidine nucleobase analogue for probing RNA structures and dynamics, comparable to fluorescent cytidine analogues.[34] Moreover, our experiments manifest the value of GNA as simple, programmable and predictable xenobiotic nucleic acid (XNA)[35] for engineering exciton coupling and transport. The demonstrated control over exciton coupling by the helical supramolecular environment provides a starting point for the elucidation of the photodynamic nature of larger BAM aggregates in nucleic acids, and may stimulate their use for photonic and fluorescent nucleic acid nanoarchitectures.

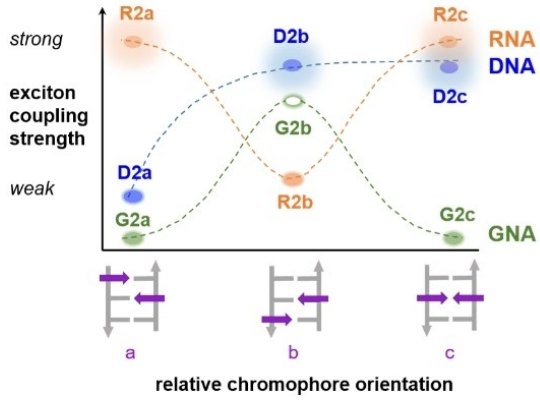

Figure 7. Schematic summary of the orientation dependence of exciton coupling strengths (*y*-axis) and folding-induced fluorescence enhancement (circles with shadows, **R2a**/**c**, **D2b**/**c**) or folding-induced fluorescence quenching (empty symbol, **G2b**) found in BAM-dimer containing double helix environments with RNA, DNA and GNA backbones.

Acknowledgements

This work was supported by the Bavarian State Ministry of Science and the Arts by establishing the Key Laboratory for Sequence-specific Polymers of the Bavarian Polymer Institute at the University of Würzburg and by the ERC (grant no. 682586). We thank Irene Bessi for recording imino proton NMR spectra. The CPL/CD hybrid spectrometer was funded by the Deutsche Forschungsgemeinschaft (DFG, German Research Foundation, grant no. 444286426). Open Access funding enabled and organized by Projekt DEAL.

Conflict of Interest

The authors declare no conflict of interest.

Data Availability Statement

The data that support the findings of this study are available in the Supporting Information of this article.

Keywords: Chromophore assembly · Merocyanine · Nucleic acids · Nucleobase analogue · Supramolecular element

[1] a) W. Xu, K. M. Chan, E. T. Kool, *Nat. Chem.* **2017**, *9*, 1043–1055; b) M. Bood, S. Sarangamath, M. S. Wranne, M. Grotli, L. M. Wilhelmsson, *Beilstein J. Org. Chem.* **2018**, *14*, 114–129.
[2] a) S. Berndl, H. A. Wagenknecht, *Angew. Chem. Int. Ed.* **2009**, *48*, 2418–2421; *Angew. Chem.* **2009**, *121*, 2454–2457; b) S. Berndl, S. D. Dimitrov, F. Menacher, T. Fiebig, H. A. Wagen-

knecht, *Chem. Eur. J.* **2016**, *22*, 2386–2395; c) S. Berndl, M. Breunig, A. Gopferich, H. A. Wagenknecht, *Org. Biomol. Chem.* **2010**, *8*, 997–999; d) V. Karunakaran, J. L. Perez Lustres, L. Zhao, N. P. Ernsting, O. Seitz, *J. Am. Chem. Soc.* **2006**, *128*, 2954–2962; e) T. Takada, K. Nishida, Y. Honda, A. Nakano, M. Nakamura, S. Fan, K. Kawai, M. Fujitsuka, K. Yamana, *ChemBioChem* **2021**, *22*, 2729–2735.

[3] F. Hövelmann, I. Gaspar, A. Ephrussi, O. Seitz, *J. Am. Chem. Soc.* **2013**, *135*, 19025–19032.

[4] C. Holzhauser, H.-A. Wagenknecht, *J. Org. Chem.* **2013**, *78*, 7373–7379.

[5] a) E. V. Dolgosheina, P. J. Unrau, *Wiley Interdiscip. Rev. RNA* **2016**, *7*, 843–851; b) R. Micura, C. Höbartner, *Chem. Soc. Rev.* **2020**, *49*, 7331–7353.

[6] a) R. X. Ren, N. C. Chaudhuri, P. L. Paris, S. Rumney, E. T. Kool, *J. Am. Chem. Soc.* **1996**, *118*, 7671–7678; b) F. Wojciechowski, J. Lietard, C. J. Leumann, *Org. Lett.* **2012**, *14*, 5176–5179; c) N. A. Grigorenko, C. J. Leumann, *Chem. Eur. J.* **2009**, *15*, 639–645.

[7] C. Brotschi, G. Mathis, C. J. Leumann, *Chem. Eur. J.* **2005**, *11*, 1911–1923.

[8] S. Hainke, O. Seitz, *Angew. Chem. Int. Ed.* **2009**, *48*, 8250–8253; *Angew. Chem.* **2009**, *121*, 8399–8402.

[9] S. Li, S. M. Langenegger, R. Häner, *Chem. Commun.* **2013**, *49*, 5835–5837.

[10] a) D. Baumstark, H. A. Wagenknecht, *Angew. Chem. Int. Ed.* **2008**, *47*, 2612–2614; *Angew. Chem.* **2008**, *120*, 2652–2654; b) P. P. Neelakandan, T. A. Zeidan, M. McCullagh, G. C. Schatz, J. Vura-Weis, C. H. Kim, M. R. Wasielewski, F. D. Lewis, *Chem. Sci.* **2014**, *5*, 973–981; c) D. Baumstark, H. A. Wagenknecht, *Chem. Eur. J.* **2008**, *14*, 6640–6645.

[11] a) L. I. Markova, V. L. Malinovskii, L. D. Patsenker, R. Häner, *Chem. Commun.* **2013**, *49*, 5298–5300; b) A. Fegan, P. S. Shirude, S. Balasubramanian, *Chem. Commun.* **2008**, 2004–2006; c) B. L. Cannon, D. L. Kellis, L. K. Patten, P. H. Davis, J. Lee, E. Graugnard, B. Yurke, W. B. Knowlton, *J. Phys. Chem. A* **2017**, *121*, 6905–6916.

[12] a) L. I. Markova, V. L. Malinovskii, L. D. Patsenker, R. Häner, *Org. Biomol. Chem.* **2012**, *10*, 8944–8947; b) O. A. Mass, C. K. Wilson, S. K. Roy, M. S. Barclay, L. K. Patten, E. A. Terpetschnig, J. Lee, R. D. Pensack, B. Yurke, W. B. Knowlton, *J. Phys. Chem. B* **2020**, *124*, 9636–9647.

[13] L. A. Fendt, I. Bouamaied, S. Thoni, N. Amiot, E. Stulz, *J. Am. Chem. Soc.* **2007**, *129*, 15319–15329.

[14] a) M. Vybornyi, Y. Vyborna, R. Häner, *Chem. Soc. Rev.* **2019**, *48*, 4347–4360; b) P. Ensslen, H. A. Wagenknecht, *Acc. Chem. Res.* **2015**, *48*, 2724–2733.

[15] a) F. Nicoli, M. K. Roos, E. A. Hemming, M. D. Antonio, R. d. Vivie-Riedle, T. Liedl, *J. Phys. Chem. A* **2016**, *120*, 9941–9947; b) S. M. Hart, W. J. Chen, J. L. Banal, W. P. Bricker, A. Dodin, L. I. Markova, Y. Vyborna, A. P. Willard, R. Häner, M. Bathe, G. S. Schlau-Cohen, *Chem* **2021**, *7*, 752–773.

[16] a) F. Würthner, *Acc. Chem. Res.* **2016**, *49*, 868–876; b) E. Kirchner, D. Bialas, F. Fennel, M. Grüne, F. Würthner, *J. Am. Chem. Soc.* **2019**, *141*, 7428–7438; c) D. Bialas, A. Zitzler-Kunkel, E. Kirchner, D. Schmidt, F. Würthner, *Nat. Commun.* **2016**, *7*, 12949.

[17] S. Yao, U. Beginn, T. Gress, M. Lysetska, F. Würthner, *J. Am. Chem. Soc.* **2004**, *126*, 8336–8348.

[18] a) X. Hu, J. O. Lindner, F. Würthner, *J. Am. Chem. Soc.* **2020**, *142*, 3321–3325; b) X. Hu, A. Schulz, J. O. Lindner, M. Grüne, D. Bialas, F. Würthner, *Chem. Sci.* **2021**, *12*, 8342–8352.

[19] a) A. T. Johnson, M. K. Schlegel, E. Meggers, L.-O. Essen, O. Wiest, *J. Org. Chem.* **2011**, *76*, 7964–7974; b) M. K. Schlegel, L.-O. Essen, E. Meggers, *J. Am. Chem. Soc.* **2008**, *130*, 8158–8159.

[20] E. Meggers, L. Zhang, *Acc. Chem. Res.* **2010**, *43*, 1092–1102.

[21] H. W. Schmidt, F. Würthner, *Angew. Chem. Int. Ed.* **2020**, *59*, 8766–8775; *Angew. Chem.* **2020**, *132*, 8846–8856.

[22] a) A. V. Kulinich, N. A. Derevyanko, A. A. Ishchenko, *Russ. J. Gen. Chem.* **2006**, *76*, 1441–1457; b) B. R. Cho, J. T. Je, S. J. Lee, S. H. Lee, H. S. Kim, S. J. Jeon, O. K. Song, C. H. Wang, *J. Chem. Soc. Perkin Trans. 2* **1996**, 2141–2144.

[23] a) B. Samanta, J. Seikowski, C. Höbartner, *Angew. Chem. Int. Ed.* **2016**, *55*, 1912–1916; *Angew. Chem.* **2016**, *128*, 1946–1950; b) S. Haag, K. E. Sloan, N. Ranjan, A. S. Warda, J. Kretschmer, C. Blessing, B. Hubner, J. Seikowski, S. Dennerlein, P. Rehling, M. V. Rodnina, C. Höbartner, M. T. Bohnsack, *EMBO J.* **2016**, *35*, 2104–2119.

[24] a) L. J. Prins, C. Thalacker, F. Würthner, P. Timmerman, D. N. Reinhoudt, *Proc. Natl. Acad. Sci. USA* **2001**, *98*, 10042–10045; b) F. Würthner, S. Yao, B. Heise, C. Tschierske, *Chem. Commun.* **2001**, 2260–2261; c) F. Würthner, J. Schmidt, M. Stolte, R. Wortmann, *Angew. Chem. Int. Ed.* **2006**, *45*, 3842–3846; *Angew. Chem.* **2006**, *118*, 3926–3930; d) J. Schmidt, R. Schmidt, F. Würthner, *J. Org. Chem.* **2008**, *73*, 6355–6362.

[25] a) S. Datta, Y. Kato, S. Higashiharaguchi, K. Aratsu, A. Isobe, T. Saito, D. D. Prabhu, Y. Kitamoto, M. J. Hollamby, A. J. Smith, R. Dalgliesh, N. Mahmoudi, L. Pesce, C. Perego, G. M. Pavan, S. Yagai, *Nature* **2020**, *583*, 400–405; b) K. Aratsu, R. Takeya, B. R. Pauw, M. J. Hollamby, Y. Kitamoto, N. Shimizu, H. Takagi, R. Haruki, S. I. Adachi, S. Yagai, *Nat. Commun.* **2020**, *11*, 1623.

[26] a) K. Schlegel, E. Meggers, *J. Org. Chem.* **2009**, *74*, 476–482; b) L. Zhang, A. E. Peritz, P. J. Caroll, E. Meggers, *Synthesis* **2006**, 645–653.

[27] T. Fujii, M. Urushihara, H. Kashida, H. Ito, X. Liang, M. Yagi-Utsumi, K. Kato, H. Asanuma, *Chem. Eur. J.* **2012**, *18*, 13304–13313.

[28] a) D. Bialas, E. Kirchner, F. Würthner, *Chem. Commun.* **2016**, *52*, 3777–3780; b) E. Kirchner, D. Bialas, M. Wehner, D. Schmidt, F. Würthner, *Chem. Eur. J.* **2019**, *25*, 11285–11293.

[29] S. H. Sohail, J. P. Otto, P. D. Cunningham, Y. C. Kim, R. E. Wood, M. A. Allodi, J. S. Higgins, J. S. Melinger, G. S. Engel, *Chem. Sci.* **2020**, *11*, 8546–8557.

[30] F. C. Spano, *Acc. Chem. Res.* **2010**, *43*, 429–439.

[31] a) J. Shi, M. A. Izquierdo, S. Oh, S. Y. Park, B. Milian-Medina, D. Roca-Sanjuan, *Org. Chem. Front.* **2019**, *6*, 1948–1954; b) J. Hoche, A. Schulz, L. M. Dietrich, A. Humeniuk, M. Stolte, D. Schmidt, T. Brixner, F. Würthner, R. Mitric, *Chem. Sci.* **2019**, *10*, 11013–11022.

[32] H. Kashida, K. Nishikawa, Y. Ito, K. Murayama, I. Hayashi, T. Kakuta, T. Ogoshi, H. Asanuma, *Chem. Eur. J.* **2021**, *27*, 14582–14585.

[33] a) D. C. Ward, E. Reich, L. Stryer, *J. Biol. Chem.* **1969**, *244*, 1228–1237; b) M. F. Soulière, A. Haller, R. Rieder, R. Micura, *J. Am. Chem. Soc.* **2011**, *133*, 16161–16167.

[34] a) A. F. Füchtbauer, S. Preus, K. Borjesson, S. A. McPhee, D. M. J. Lilley, L. M. Wilhelmsson, *Sci. Rep.* **2017**, *7*, 2393; b) M. Bood, A. W. Del Nogal, J. R. Nilsson, F. Edfeldt, A. Dahlen, M. Lemurell, L. M. Wilhelmsson, M. Grotli, *Sci. Rep.* **2021**, *11*, 9396.

[35] K. Murayama, H. Asanuma, *ChemBioChem* **2021**, *22*, 2507–2515.

Manuscript received: December 8, 2021
Accepted manuscript online: December 22, 2021
Version of record online: ■■, ■■

Research Articles

Oligonucleotides

J. Dietzsch, D. Bialas, J. Bandorf,
F. Würthner,*
C. Höbartner* _____ **e202116783**

Tuning Exciton Coupling of Merocyanine Nucleoside Dimers by RNA, DNA and GNA Double Helix Conformations

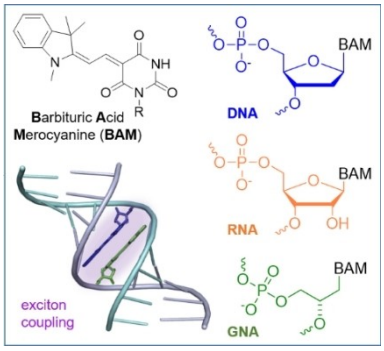

The barbituric acid merocyanine (BAM) is reported as a nucleobase surrogate that forms hydrogen-bonded base pairs, and antiparallel as well as rotationally stacked dimer aggregates, with orientation- and conformation-sensitive exciton coupling strength.